

A New Delayed Resonator Design Approach for Extended Operable Frequency Range

Oytun Eris

AVL Turkey

Abdurrahmangazi Mah. Ataturk Cad. 22, 34920, Istanbul, TURKEY

erisoy@itu.edu.tr

Baran Alikoc*

Czech Institute of Informatics, Robotics, and Cybernetics,

Czech Technical University in Prague, 160 00 Prague, Czech Republic

baran.alikoc@cvut.cz

Ali Fuat Ergenc¹

Istanbul Technical University

Control and Automation Eng. Dept., 34469, Istanbul, TURKEY

ergenca@itu.edu.tr

ABSTRACT

The operable frequency range of the Delayed Resonators (DR) is known to be narrow due to stability issues. This study presents a novel approach for DR design with a combined feedback strategy that consists of a delayed velocity and non-delayed position feedback to extend the operable frequency range of the DR method. The non-delayed position feedback is used to alter the natural frequency of the DR artificially while delayed velocity feedback is employed to tune the frequency of DR matching with the undesired vibrations. The proposed method also introduces an optimization parameter that provides freedom for the designer to obtain fast vibration suppression while improving the stability range of the DR. An

¹ Corresponding Author

* The author conducted this research in part while he was with Control and Automation Eng. Dept., Istanbul Technical University.

optimization approach is also provided within the scope of this study. Theoretical findings are verified over an experiment utilizing the active suspension system of the Quanser® Company.

1. INTRODUCTION

The Delayed Resonator (DR), an active vibration absorption technique, has been influential since their introduction by Olgac and Holm-Hansen [1]. The principal idea behind the DR is to obtain a pure resonator with a simple mass-spring-damper system that oscillates at the same frequency of the undesired vibrations. The resonator is tuned using partial state feedback with time delay. The vibrations with this specific frequency on the primary structure are suppressed by the oscillation of the DR. Implementations of the classical DRs are made by utilizing a delayed position [2], acceleration [3, 17, 18] or velocity [4] feedback depending on the type of sensor used in the application.

There are numerous studies on the DRs that are focused on the different aspects of the method since 1990s. The DR design with delayed position feedback is investigated in [5], the concept of dual frequency suppression with single mass is examined in [6, 7]. Furthermore, auto-tuning mechanisms [8-10] are proposed to extend the stable operation range of the DR method against changing parameters and vibration frequencies. The idea of using multiple DRs on multi-degree-of-freedom systems is investigated in [11]. Aside of linear systems, the DRs are also adapted to suppress torsional vibrations by using delayed velocity feedback in [12, 13]. In a recent study [14], the DR concept is also applied to obtain enhanced energy harvesting. The utilization of the DRs is also considered for different problems such as machine chattering

applications [15] and active vehicle suspension [4, 16], rather than only vibration absorption.

Although the DR implementation is very simple, maintaining the stability against varying operation frequencies is a major drawback. There are several auto-tuning algorithms proposed in the literature but still, the operable frequency range of a DR is limited to its physical parameters and feedback type due to stabilization issues. A complete stability analysis of the DR with acceleration and velocity feedback is addressed in [17] and [18]. Beside the stability of the DR, stability of the *coupled system* (CS), DR and the primary structure together, under varying operational conditions should also be taken into consideration. Some studies on different feedback strategies for extended operation range are studied in [18] and [19].

The aim of this paper is to introduce a new modified approach to the classical DR concept to extend the operable frequency range of the resonator. Thus, proposition and experimental verification of a combined feedback controller strategy that consists of a delayed velocity and non-delayed position feedback which enhances the frequency range of suppression are the main contributions of this study. The proposed method provides the designer to choose the gain of the position feedback freely while the gain and the delay parameters of the velocity feedback are determined analytically with respect to the position gain and the frequency subject to be suppressed. An optimization methodology for the determination of this free gain parameter is proposed to achieve fast vibration suppression as well as improving the stability range with respect to the excitation frequency of both DR and CS.

In the following section, preliminaries on DRs and the motivation of this study is presented. For the sake of the clarity, first we introduce the model with real parameters. The proposed feedback strategy is explained including dimensionless model in Section 3, while Section 4 is dedicated to the stability analysis. Finally, experimental verification of the proposed approach is provided in Section 5 and concluding remarks are given in Section 6.

2. PRELIMINARIES AND MOTIVATION

Preliminaries

A classical DR attached to a SDOF (single degree-of-freedom) primary system is depicted in Fig. 1. In the DR method, it is aimed to obtain a pure resonator which is tuned to the frequency of the vibrations produced by the external force $f(t)$. Tuning is attained by the control effort

$$u(t) = g_c x_a(t - \tau_c) \quad (1)$$

which consists of a feedback gain g_c and artificially introduced feedback delay τ_c in the position state x_a [1]. The motion equation of the DR is given by

$$m_a \ddot{x}_a(t) + c_a \dot{x}_a(t) + k_a x_a(t) = u(t) \quad (2)$$

where m_a is the DR mass and k_a, c_a are the stiffness and damping coefficients of the DR, respectively. The characteristic polynomial of the DR is given as

$$CE(s) = m_a s^2 + c_a s + k_a - g_c e^{-s\tau_c}. \quad (3)$$

The feedback gain and the delay parameters which places the dominant pair of the infinitely many characteristic roots of the DR onto the desired $\mp \omega i$ on imaginary axis,

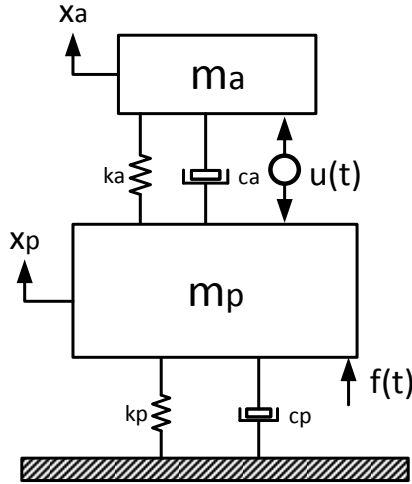


Figure 1. Delayed Resonator vibration absorber attached to a SDOF primary system.

where ω is the excitation frequency of the force $f(t)$ applied to the primary system, are derived as

$$g_c = \mp \sqrt{(c_a \omega)^2 + (m_a \omega^2 - k_a)^2}$$

$$\tau_c = \frac{1}{\omega} \left\{ \tan^{-1} \left[\frac{c_a \omega}{m_a \omega^2 - k_a} \right] + 2(l-1)\pi \right\} \text{ for } l = 1, 2, \dots \quad (4)$$

It is obvious from the equations that for each g_c there are multiple corresponding values of τ_c depending on the **delay-gain branch** number l .

Note that, although two of the characteristic roots of the DR are placed on $\mp \omega i$ and at resonance for each case, the CS performs differently depending to the branch number and the feedback type. This behavior is due the effect of the other infinitely many roots that are moving closer to the imaginary axis by the increasing time delay and dictating the response.

Let us remark that the formulas of the gain and delay parameters for the control laws with delayed velocity feedback, i.e. $x_a \rightarrow \dot{x}_a$ in (1), and the acceleration feedback, i.e. $x_a \rightarrow \ddot{x}_a$ in (1), have been also derived in [3,4,17,18].

Motivation

The performance of the DRs is susceptible against the change in frequency of the vibrations. Since it is not achievable to adjust the physical parameters of the DR during operation, auto-tuning methods that update the controller parameters are proposed [8-10]. Unfortunately, as the difference between the natural frequency ($\Omega = \sqrt{k_a/m_a}$) of the DR and the excitation frequency ω of the external force $f(t)$ increases, stability issues arise both for the DR and the CS which restricts the efficiency of these methods within a small frequency range. Interestingly, without changing any physical parameters this frequency range can be altered by selecting a different delay-gain branch number or feedback type.

To validate our claim, let us consider the system with the parameters $m_p = 10 \text{ kg}$, $c_p = 500 \text{ kg s}^{-1}$, $k_p = 3000 \text{ N m}^{-1}$, $m_a = 1 \text{ kg}$, $c_a = 12.05 \text{ kg s}^{-1}$, $k_a = 908 \text{ N m}^{-1}$ which was studied in [17]. We perform the stability analysis of this system numerically by computing the rightmost roots of the DR and the CS for different feedback laws and delay branches, utilizing the methods in [20,21]. Stability posture for the DR and CS are presented in Fig. 2, with normalized vibration frequency with respect to the natural frequency of the DR ($\bar{\omega} = \omega/\Omega$). Note that, for a successful suppression, the real part of the DR's rightmost root, i.e. spectral abscissa, is expected to be zero while the rightmost root of the CS must lie on the left half plane (LHP) for stability.

The stability ranges of DR's for the first branches ($l = 1$) of acceleration ($\bar{\omega}: 0.79 - \infty$) and position feedback ($\bar{\omega}: 1.0 - \infty$) are unbounded from above as depicted in Fig. 2. On the other hand, the first branch of the velocity feedback ($\bar{\omega}: 0.512 - 1.0$) is bounded

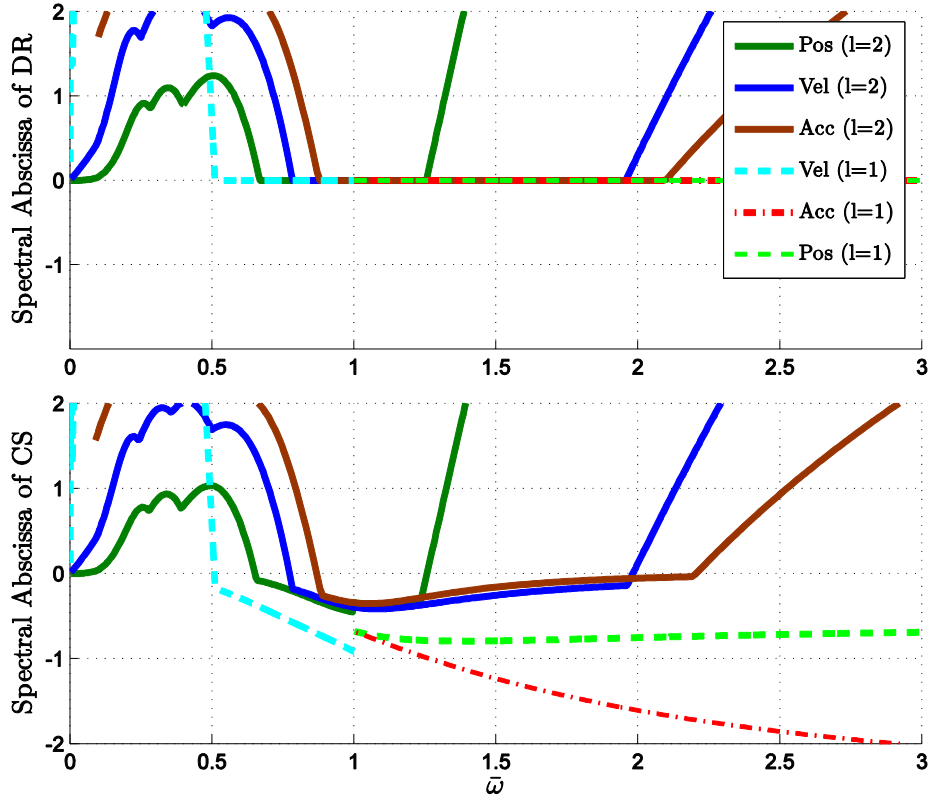


Figure 2. Spectral abscissa of the DR and CS with respect to changing excitation frequency.

from above since the computed τ_c values w.r.t. the suppression frequencies (ω) become negative which are physically not applicable. Note that, the second delay branch ($l = 2$) of the velocity feedback ($\bar{\omega}: 0.784 - 1.956$) provides a wider stability range comparing to the first branch while the second branches display reduced stability ranges for the position ($\bar{\omega}: 0.669 - 1.254$) and acceleration ($\bar{\omega}: 0.876 - 2.096$ Hz) feedbacks.

Although the DR design is independent of the primary system parameters (m_p, c_p, k_p), stability of the CS, which is not studied deeply in the literature and it should be taken into consideration during the design. The stability range of the CS might be narrower than the DR's stability range which is affected by the primary system parameters. Analyzing further on the previous example, the effect of the primary system's damping ratio ($\zeta_p = c_p/2\sqrt{m_p k_p}$) on the CS's stability is depicted in Fig. 3 for different feedback types and delay branches utilizing spectral abscissa computation with numerical methods described in [21].

The stability posture of the CS for the position feedback DR case is presented in the Fig. 3(a) and Fig 3(b). The frequency range of the stable operation of the CS is almost same with the DR's stability range for all the damping ratio values ($\bar{\omega}$: 1.0 – ∞) except $\zeta_p = 0.01$ which has a higher lower bound ($\bar{\omega}$: 1.142 – ∞) for the first delay branch,. On the other hand, the effects of lower damping values on the stable operation range is more apparent for the second delay branch of the position feedback; the stability range for ω is quite narrower.

The stable operation ranges for the second delay branch of the velocity feedback are constricted for smaller damping ratio of the primary system as displayed in the Fig. 3(c) and Fig. 3(d). Interestingly, while the CS is unstable for $\zeta_p = 0.01$ on the first delay branch, stable operation is possible on the second delay branch.

As observed from the Fig. 3(e) and Fig. 3(f), stable operation range is remarkably reduced for the underdamped systems on the second delay branch of the acceleration

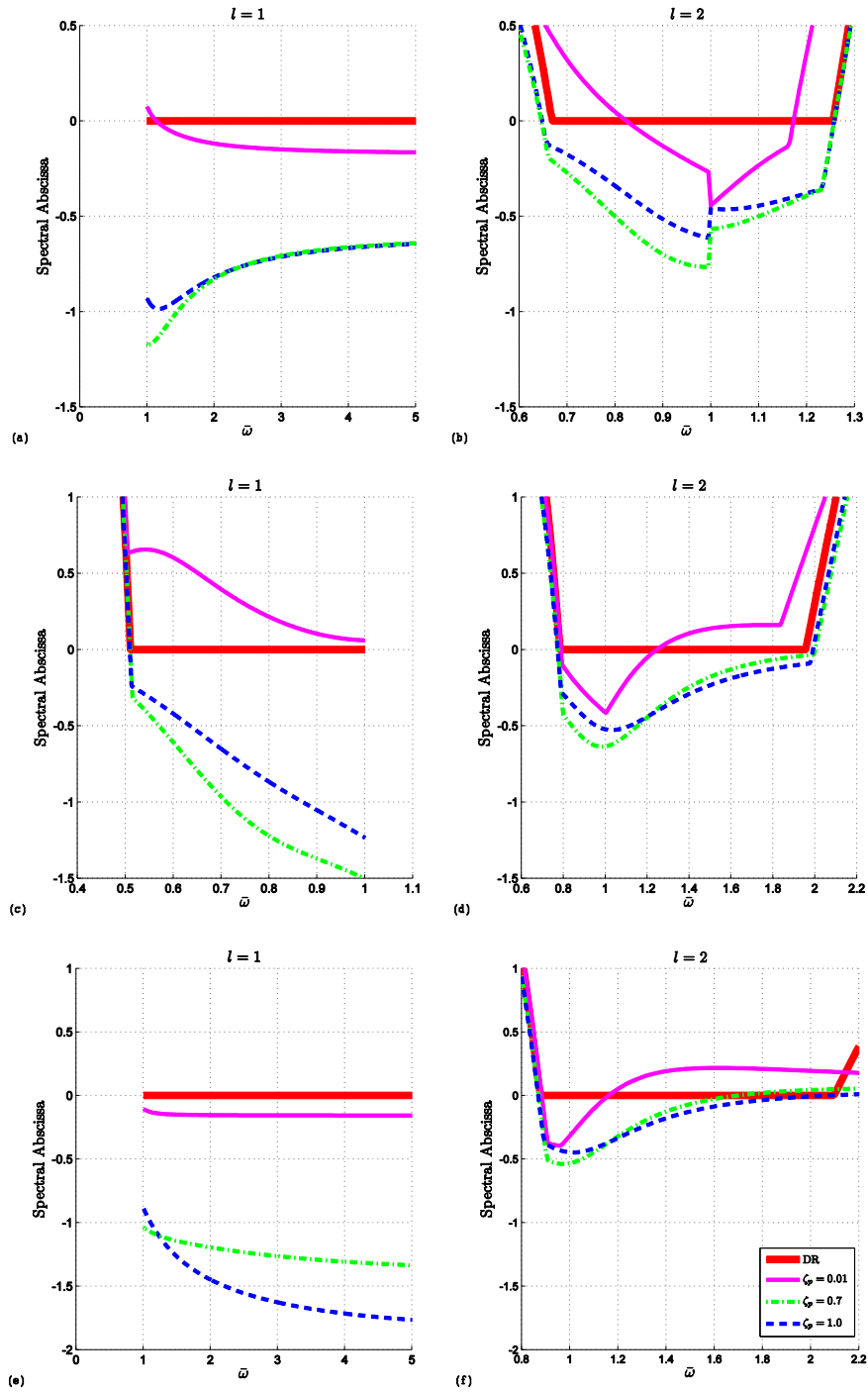


Figure 3. Spectral abscissas for different ζ_p values w.r.t. changing ω (a: Position feedback $l = 1$, b: Position feedback $l = 2$, c: Velocity feedback $l = 1$, d: Velocity feedback $l = 2$, e: Acceleration feedback $l = 1$, f: Acceleration feedback $l = 2$).

feedback. Contrary, for the first delay branch the stable operation range of the CS is almost equal to the DR's stability range except $\zeta_p = 0.01$.

Considering the fact that physical parameters of the DR are almost unalterable during the operation, a new approach to the classical DR method is necessary to extend the operable frequency range of the DR which is limited by physical constraints and stability issues. Motivation of this study is to extend the stable operation range of the method proposing a different feedback strategy to utilize the DR.

3. PROPOSED DR DESIGN METHOD

Physical parameters of the DR are usually selected such that the natural frequency of the DR is approximately same with the frequency of the undesired oscillations which are aimed to be suppressed. Sustaining the stability of the DR is challenging as the frequency of the vibrations diverges from the natural frequency of the DR. As a solution to this problem, a combined feedback control approach that consists of a position and delayed velocity feedback as

$$u(t) = g_v \dot{x}_a(t - \tau) + g_p x_a(t) \quad (5)$$

is proposed to design the DR. The purpose of the newly added position feedback with the gain (g_p) is to change the natural frequency of the DR artificially while the velocity feedback gain (g_v) and time delay are used to tune the DR to oscillate at the desired frequency. Thus, a wider frequency range for stable operation is attainable for both the DR and the CS. The dimensionless model for the DR is derived to reduce the number of the parameters and to generalize the results with respect to the natural frequency of

the DR following the procedure in [17]. The governing equation of the DR with the proposed feedback architecture in (5), is

$$m_a \ddot{x}_a(t) + c_a \dot{x}_a(t) + k_a x_a(t) - g_v \dot{x}_a(t - \tau) - g_p x_a(t) = 0. \quad (6)$$

Considering the natural frequency of the DR as $\Omega = \sqrt{k_a/m_a}$ and scaling the time as $\bar{t} = \Omega t$, (6) is rewritten as

$$m_a \Omega^2 \ddot{x}_a(\bar{t}) + c_a \Omega \dot{x}_a(\bar{t}) + k_a x_a(\bar{t}) - g_v \Omega \dot{x}_a(\bar{t} - \bar{\tau}) - g_p x_a(\bar{t}) = 0 \quad (7)$$

where $\bar{\tau} = \Omega \tau$. Defining the damping ratio of the absorber as $\zeta = c_a/2\sqrt{k_a m_a}$ and dividing (7) by $m_a \Omega^2$, then we have

$$\ddot{x}_a(\bar{t}) + 2\zeta \dot{x}_a(\bar{t}) + x_a(\bar{t}) - \bar{g}_v \dot{x}_a(\bar{t} - \bar{\tau}) - \bar{g}_p x_a(\bar{t}) = 0 \quad (8)$$

where the velocity and position feedback gains are defined as $\bar{g}_v = g_v/\sqrt{k_a m_a}$ and $\bar{g}_p = g_p/k_a$, respectively.

The characteristic equation of the DR regarding (8) is

$$CE(s) = s^2 + 2\zeta s + 1 - \bar{g}_v s e^{-s\bar{\tau}} - \bar{g}_p. \quad (9)$$

After substituting $\bar{\omega}i$ for s where $\bar{\omega} = \omega/\sqrt{k_a/m_a}$, the characteristic equation is split to the real and imaginary parts as

$$\begin{aligned} Re\{CE(j\bar{\omega})\} &= -\bar{\omega}^2 + 1 - \bar{g}_p + \bar{g}_v \bar{\omega} \sin(\bar{\omega}\bar{\tau}) \\ Im\{CE(j\bar{\omega})\} &= 2\zeta \bar{\omega} - \bar{g}_v \bar{\omega} \cos(\bar{\omega}\bar{\tau}). \end{aligned} \quad (10)$$

Considering \bar{g}_p as a free parameter, the velocity feedback gain and the delay that satisfy $Re\{CE(j\bar{\omega})\} = 0$ and $Im\{CE(j\bar{\omega})\} = 0$ to assign the dominant roots of the DR on the imaginary axis ($\mp \bar{\omega}i$) are

$$\bar{g}_v = \frac{1}{\bar{\omega}} \sqrt{(2\zeta \bar{\omega})^2 + (1 - \bar{\omega}^2 - \bar{g}_p)^2} \quad (11)$$

$$\bar{\tau} = \frac{1}{\bar{\omega}} \left\{ \text{atan2} \left[\frac{1 - \bar{\omega}^2 - \bar{g}_p}{2\zeta\bar{\omega}} \right] + 2(l-1)\pi \right\}, \quad l = 1, 2 \dots$$

The position feedback gain is freely selected to alter the natural frequency of the DR by changing the DR's stiffness artificially. Thus, the position feedback gain is proposed as

$$\bar{g}_p = 1 - \alpha\bar{\omega}^2. \quad (12)$$

where α is the tuning parameter that might be used for optimization purposes. Note that the selection of α will be explained in a different subsection.

Obviously, for $\alpha = 1$ the natural frequency of the DR coincides with the frequency of the vibrations which leads to a zero delay case if the first delay branch is selected where $\bar{\tau} = 0$ and $\bar{g}_v = 2\zeta$. Naturally, for the zero delay case some stability issues may arise for the CS depending on the physical parameters (See Remark 4). This stability problem may be solved by selecting higher delay branches. Here, we wish to indicate the relation of our study to a delay-free absorber to the DR proposed in [25] where a PI acceleration feedback is considered. The proposed feedback gain (12) with $\alpha = 1$ yields a PD position feedback without delay when $l = 1$ is chosen. Our approach makes a step forward with respect to [25] by considering a different feedback architecture and extending it with the delayed case.

Dimensionless model may also be extended for the CS using the same approach.

Defining $\bar{m}_p = m_p/m_a$, $\bar{c}_p = c_p/m_a\Omega$, $\bar{k}_p = k_p/m_a\Omega^2$ and $\bar{f}(\bar{t}) = f(t)/m_a\Omega^2$ dynamic equations of the CS are

$$\ddot{x}_a(\bar{t}) + 2\zeta\dot{x}_a(\bar{t}) + x_a(\bar{t}) - \bar{g}_v\dot{x}_a(\bar{t} - \bar{\tau}) - \bar{g}_p x_a(\bar{t}) = 2\zeta\dot{x}_p(\bar{t}) + x_p(\bar{t}), \quad (13)$$

$$\begin{aligned} \bar{m}_p \ddot{x}_p(\bar{t}) + (2\zeta + \bar{c}_p) \dot{x}_p(\bar{t}) + (1 + \bar{k}_p) x_p(\bar{t}) \\ = 2\zeta \dot{x}_a(\bar{t}) + x_a(\bar{t}) - \bar{g}_v \dot{x}_a(\bar{t} - \bar{\tau}) - \bar{g}_p x_a(\bar{t}) + \bar{f}(\bar{t}) \end{aligned} \quad (14)$$

By defining the state vector as $x = [x_a \quad \dot{x}_a \quad x_p \quad \dot{x}_p]^T$, the state space representation of (13) and (14) are obtained as

$$\dot{x}(\bar{t}) = Ax(\bar{t}) + A_T x(\bar{t} - \bar{\tau}) + B\bar{f}(\bar{t}) \quad (15)$$

where

$$A = \begin{bmatrix} 0 & 1 & 0 & 0 \\ -1 + \bar{g}_p & -2\zeta & 1 & 2\zeta \\ 0 & 0 & 0 & 1 \\ \frac{1 + \bar{g}_p}{\bar{m}_p} & \frac{2\zeta}{\bar{m}_p} & -\frac{1 + \bar{k}_p}{\bar{m}_p} & -\frac{2\zeta + \bar{c}_p}{\bar{m}_p} \end{bmatrix}, A_T = \begin{bmatrix} 0 & 0 & 0 & 0 \\ 0 & \bar{g}_v & 10 & 0 \\ 0 & 0 & 0 & 0 \\ 0 & -\frac{\bar{g}_v}{\bar{m}_p} & 0 & 0 \end{bmatrix}, B = \begin{bmatrix} 0 \\ 0 \\ 0 \\ 1 \\ \bar{m}_p \end{bmatrix}. \quad (16)$$

Remark 1: Since the delay parameter values regarding the first delay branch for $\alpha < 1$ are negative, higher delay branches ($l > 1$) must be selected for application in case $\alpha < 1$.

Remark 2: The value of the delay parameter $\bar{\tau}$ decrease rapidly as the frequency of the vibrations increase as it is seen from (11). Therefore, an upper bound for the operation frequency will be imposed since it is necessary for the sampling period of the implementation hardware to be much smaller than the delay parameter ($t_s \ll \bar{\tau}$). Upper delay branches can be considered for higher frequencies.

Selection of the optimization parameter α

The parameter α of the proposed control scheme changes the stiffness between the principle mass and the DR. The change in the stiffness naturally affects the location of the spectral abscissa of the CS which defines the transient response of the overall

structure. The farther left the rightmost root is assigned, faster vibration suppression is achieved. Hence, optimization using α parameter for a farthestmost spectral abscissa of the CS is beneficial for better control performance. Characteristic roots of the CS are obtained from the characteristic equation

$$\det(sI - A - A_T e^{s\bar{\tau}}) = 0. \quad (17)$$

Considering $\lambda_1, \dots, \lambda_\infty$ are the characteristic roots of (17), the objective of the optimization is to minimize the spectral abscissa of the CS, for each frequency within the desired operation range, subject to α which regards to the performance index

$$\min_{\alpha} \left\{ \max_{1 \leq i < \infty} \{Re(\lambda_i)\} \right\}. \quad (18)$$

Note that, for stable operation the spectral abscissa of the CS must be on the LHP. Considering the stability constraints, optimization can be made for a narrower α range in which the DR is stable. Therefore, the effort and time for the optimization will be significantly reduced. The optimization given by (18) can be executed by the numerical algorithm in [22] which calculates the rightmost root of a time-delay system. Namely, the rightmost root of CS is calculated for α stabilizing the DR with a sufficient resolution and α value which makes the real part of rightmost root is determined. Let us note that analysis for the effect of α on the stability of the DR is given in the following sections.

To demonstrate the fact of proposed optimization for α , the variation of the spectral abscissa of the CS presented in Motivation section ($\zeta = 0.2$), with respect to α are shown in Fig. 4 for different operation frequencies where the delay branch is chosen as $l = 2$. Optimal α values for $\bar{\omega} = 0.417$ and $\bar{\omega} = 1$ are obtained as 0.55 and 0.885 respectively.

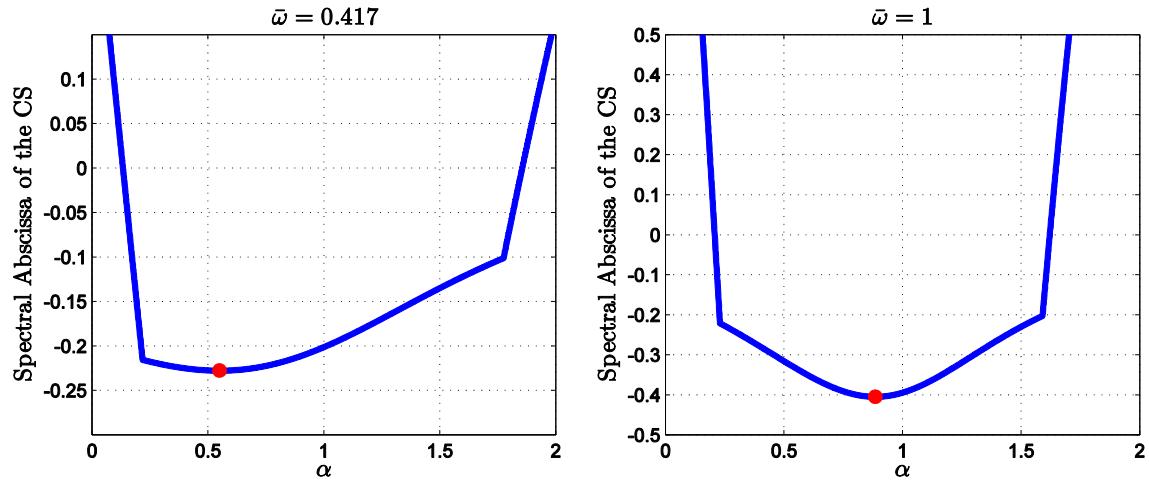


Figure 4. Change of the spectral abscissa of the CS with respect to α for $l = 2$.

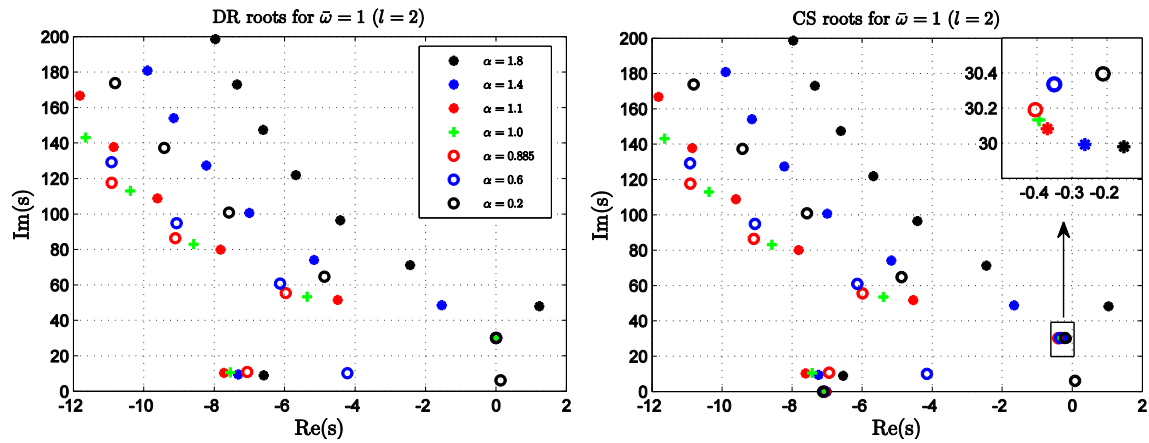


Figure 5. Root distribution of the DR and CS with respect to α for $l = 2$.

The effects of changing α values over the DR and the CS roots are demonstrated in Fig. 5 for the handled system. As depicted, although one pair of the roots is located at the desired $\bar{\omega}i$ position for all α values, the DR is unstable for $\alpha = 0.2$ and $\alpha = 1.8$ as visible from the root distribution. The farthest rightmost root position from the imaginary axis for $\bar{\omega} = 1$ is obtained for $\alpha = 0.885$ as can be observed from the root distribution of the CS, consistent with the results displayed in Fig. 5.

In the following section the stability of the DR and the CS is investigated.

4. STABILITY ANALYSIS

Stability analysis of the DR

The characteristic equation of the DR given in (9) is rearranged as,

$$s^2 + 2\zeta s + 1 - \bar{g}_p - \bar{g}_v s e^{-sv} = 0 \quad (19)$$

where $v > 0$ is the delay. The stability of the DR is studied by utilizing the Cluster Treatment of the Characteristic Roots (CTCR) methodology presented in [23]. CTCR examines the characteristic root crossings on the imaginary axis based on the Rekasius transformation [24] given by

$$e^{-sv} \rightarrow \frac{1 - Ts}{1 + Ts}, T \in \mathbb{R} \quad (20)$$

which is exact for the imaginary roots, $s = j\bar{\omega}_c$ where $\bar{\omega}_c \in \mathbb{R}^+$, with the relationship between T and $\bar{\omega}$:

$$v = \frac{2}{\bar{\omega}_c} [\tan^{-1}(\bar{\omega}_c T) + k\pi], k = 1, 2, \dots \quad (21)$$

Substituting (20) into (19), the auxiliary characteristic equation is obtained as

$$T\bar{s}^3 + (1 + 2T\zeta + T\bar{g}_v)\bar{s}^2 + (T + 2\zeta - T\bar{g}_p - \bar{g}_v)\bar{s} + (1 - \bar{g}_p) = 0. \quad (22)$$

Note that the imaginary roots of (22) are identical to the imaginary roots of (19) with the relationship (21). Thus, when the Routh's method is applied to (22), the imaginary roots $s_{1,2} = \pm j\bar{\omega}_c$ of (19) is determined from the row for s^2 of the Routh's table as

$$\bar{\omega}_c = \sqrt{\frac{1 - \bar{g}_p}{2T\zeta + T\bar{g}_v + 1}} \quad (23)$$

if

$$\frac{1 - \bar{g}_p}{2T\zeta + T\bar{g}_v + 1} > 0, \quad (24)$$

when the row for s^1 is zero satisfied by $T \in \mathbb{R}$ values

$$T_{1,2} = -\frac{\bar{g}_v^2 - 4\zeta^2 \pm \sqrt{(\bar{g}_v^2 - 4\zeta^2)(4 + \bar{g}_v^2 - 4\bar{g}_p - 4\zeta^2)}}{2(\bar{g}_p - 1)(\bar{g}_v + 2\zeta)} \quad (25)$$

if

$$(\bar{g}_v^2 - 4\zeta^2)(4 + \bar{g}_v^2 - 4\bar{g}_p - 4\zeta^2) > 0. \quad (26)$$

Once (26) is satisfied, T_p for $p = 1, 2$ are computed by (25) and then the corresponding crossing frequency, $\bar{\omega}_{cp}$, is determined by (23) when the condition (24) is satisfied.

Thereafter, the corresponding delay values are obtained using (21) as

$$v_{p,k} = \frac{2}{\bar{\omega}_{cp}} \left[\tan^{-1}(\bar{\omega}_{cp} T_p) + (k-1)\pi \right], k = 1, 2, \dots \quad (27)$$

After the delay sets yielding to the imaginary roots are computed using (27), the direction of the root migration is determined by the root tendency property,

$$RT(\bar{\omega}_{cp}, v_{p,k}) = \text{sign} \left\{ \left[\frac{\partial s}{\partial v} \Big|_{\substack{s=j\bar{\omega}_{cp} \\ v=v_{p,k}}} \right] \right\}, \quad (28)$$

which is invariant for the kernel and the offspring delay sets in the CTCR [23].

The root crossing is stabilizing when $RT(\bar{\omega}_{cp}, v_{p,k}) = -1$ and destabilizing when $RT(\bar{\omega}_{cp}, v_{p,k}) = 1$. For the characteristic equation (19) of the DR, it is examined through

$$\frac{\partial s}{\partial v} \Big|_{\substack{s=j\bar{\omega}_{cp} \\ v=v_{p,k}}} = \frac{s^2 \bar{g}_v e^{sv}}{2s + 2\zeta + e^{sv}(\bar{g}_v s v - \bar{g}_p)} \Big|_{\substack{s=j\bar{\omega}_{cp} \\ v=v_{p,k}}}. \quad (29)$$

The number of the unstable roots (NU), i.e. roots in the open right half complex plane has to be determined to assess the marginal stability of the DR (9), for the

corresponding delay value obtained using (11). It is clear that NU has to be equal to zero and only two dominant poles of DR are located on the imaginary axis for marginal stability of the DR. As an important step of the CTCR, the first NU for the zero delay case is to be known, and then NU is determined for any given delay value by the root tendency approach given particularly for the DR in (29). Note that $NU=2$ for $v = 0$ when $\alpha \neq 1$ as seen from (19). The stability posture of the DR (9) for $\zeta = 0.2$ parameterized with (11)-(12) for various α values is obtained utilizing the CTCR methodology and depicted in Fig. 6 with also respect to $\bar{\omega}$ to be suppressed. The thick green lines represent the proposed DR delay $\bar{\tau}$ for different branches l satisfying marginal stability.

Remark 3: Notice that the choice of $\alpha = 1$ provides interesting results for the proposed DR design. In this case, the position feedback gain yields $\bar{g}_p = 1 - \bar{\omega}^2$ from (12). Then, by (11), the DR is parameterized as

$$\begin{aligned} \bar{g}_v &= 2\zeta \\ \bar{\tau} &= \frac{2\pi(l-1)}{\bar{\omega}}, \quad l = 1, 2, \dots \end{aligned} \tag{30}$$

Subsequently, it is seen from (25) that $T_{1,2} = 0$ which is independent from ζ . Consequently, $v_{1,k} = v_{2,k} = 2(k-1)\pi/\bar{\omega}_c$, $k = 1, 2, \dots$, which is exactly the same as the delay parameter of the DR given in (30) since $\bar{\omega}_c = \bar{\omega}$ by (23). These results indicate the DR delay is zero for the first branch ($l = 1$) and also it is marginally stable for all the branches as shown in Fig. 6(b).

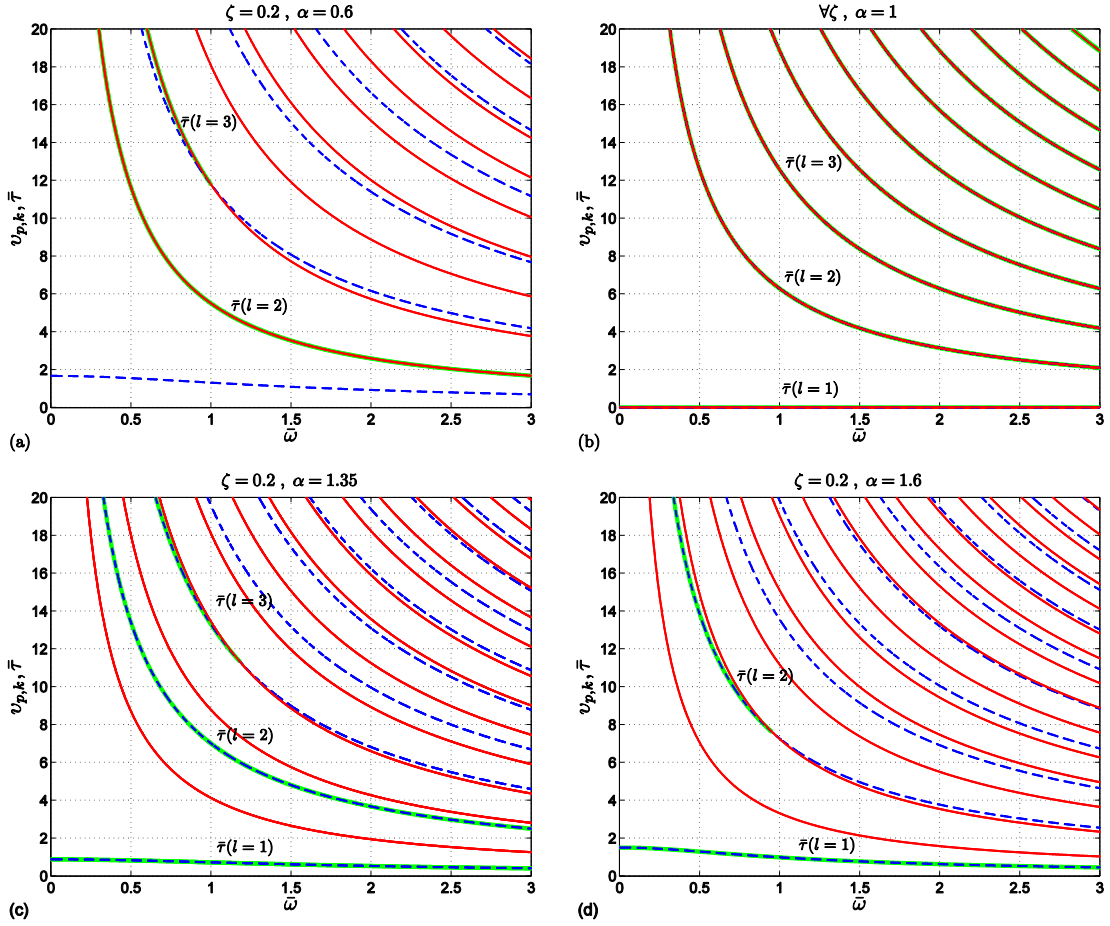


Figure 6. Stability map of DR (12) with characteristic equation (19) for $\zeta = 0.2$ and various α : (a) $\alpha = 0.6$, (b) $\alpha = 1$, (c) $\alpha = 1.35$, (d) $\alpha = 1.6$. Dashed blue lines - $v_{1,k}$ with $RT = -1$ (stabilizing), solid red lines - $v_{1,k}$ with $RT = 1$ (destabilizing), thick green lines – delay values $\bar{\tau}$ for which the DR is marginally stable.

In Fig. 7, the stability regions with respect to the free parameter α swept in the range $\alpha \in [0, 2]$, the nominal excitation frequency $\bar{\omega}$ and the delay branch number l are depicted for the given DR with $\zeta = 0.2$ by utilizing the stability analysis given above.

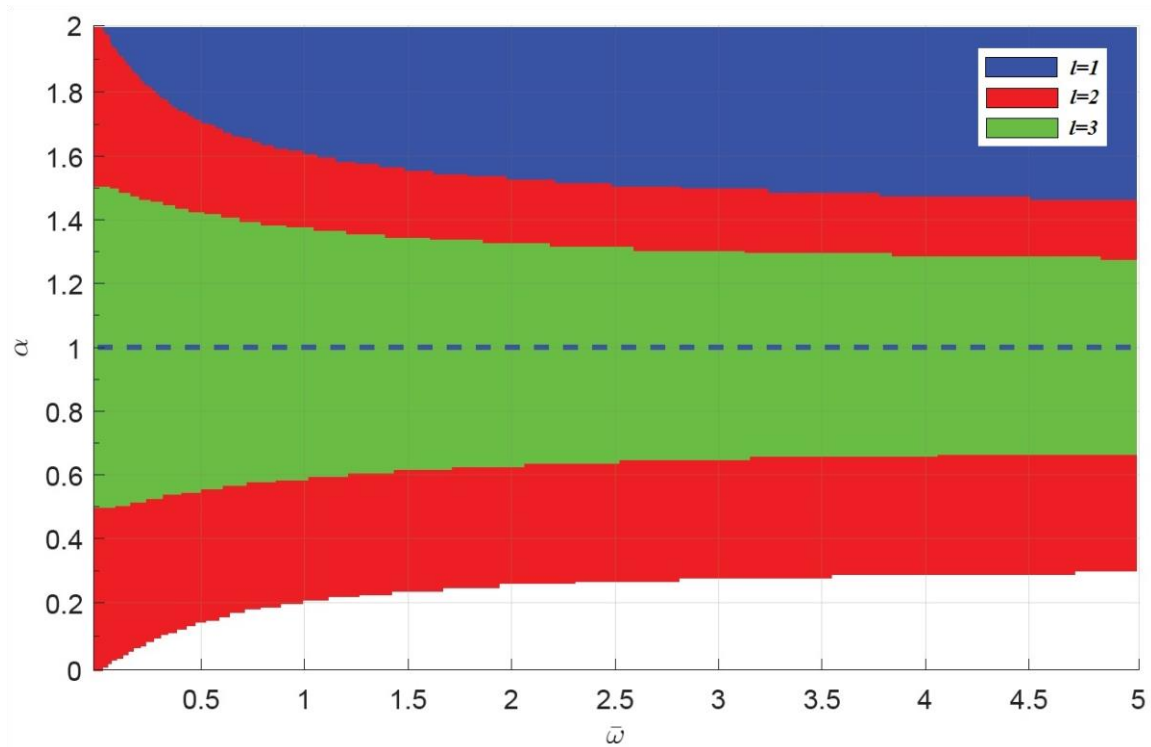


Figure 7. Stability regions of the DR with (5)-(11,12) with respect to α , $\bar{\omega}$ and l . For a given $l > 1$, the stability region is the union with the regions lying inside corresponding to the larger delay branch numbers. Dashed blue: lower applicability boundary for $l = 1$.

Note that the stable range for $(\alpha, \bar{\omega})$ gets narrower as the branch number increases. However, it is possible to choose an α value for the handled branches where DR is marginally stable for all $\bar{\omega}$ to be suppressed. This property brings an advantage comparing with the classical DR's presented in [2-4, 17, 18] since they provide bounded frequency ranges to be suppressed where the DR is marginally stable. Another advantage of the proposed DR is the availability of choosing higher branches for the DR delay parameterization when the parameterized delay value is too small to apply in real-time applications (See Remark 2).

Stability analysis of the CS

Stability analysis of the CS is performed over the characteristic equation of the system which can be obtained from (19) as

$$s^4 + \left(\frac{\bar{c}_p + 2\zeta}{\bar{m}_p} + 2\zeta - \bar{g}_v e^{s\bar{\tau}} \right) s^3 + \left(\frac{1 + \bar{k}_p + 2\bar{c}_p\zeta - \bar{c}_p\bar{g}_v e^{s\bar{\tau}}}{\bar{m}_p} + 1 - \bar{g}_p \right) s^2 + \left(\frac{\bar{c}_p(1 - \bar{g}_p) + \bar{k}_p(2\zeta - \bar{g}_v e^{s\bar{\tau}})}{\bar{m}_p} \right) s + \frac{\bar{k}_p(1 - \bar{g}_p)}{\bar{m}_p} = 0. \quad (31)$$

Due to the system order and many parameters of the CS's characteristic equation, analytical analysis of the stability is cumbersome and almost impossible to visualize with respect to the general parameters and delay. Thus, numerical methods [20] are used to analyze the effects of α and l over the stability of the CS. The spectral abscissa of the handled system ($\zeta = 0.2, \Omega = 4.7958, \bar{k}_p = 3.304, \bar{c}_p = 16,5931, \bar{m}_p = 10$) for the different values of α and l are displayed in Fig. 8 and Fig. 9, respectively.

The stability ranges for the displayed α values are unbounded except for $\alpha = 0.2$ and $\alpha = 1.8$ which are bounded from above as it is visible on Fig. 8. Results also reveal α values that provide the farthest rightmost root positions from the imaginary axis changes for different frequencies. For instance, the farthest rightmost root position for $\bar{\omega} = 0.5$ is obtained for $\alpha = 0.6$ while the farthest rightmost root position for $\bar{\omega} = 1.5$ is obtained for $\alpha = 0.885$.

Contrary to the results obtained for the classical methods that are presented in Fig. 2, the proposed method provides unbounded stability range of $\bar{\omega}$ for all the delay branches displayed in Fig. 9. Therefore, higher delay branches that provide larger τ values can be considered for higher frequencies. Another observation is that the

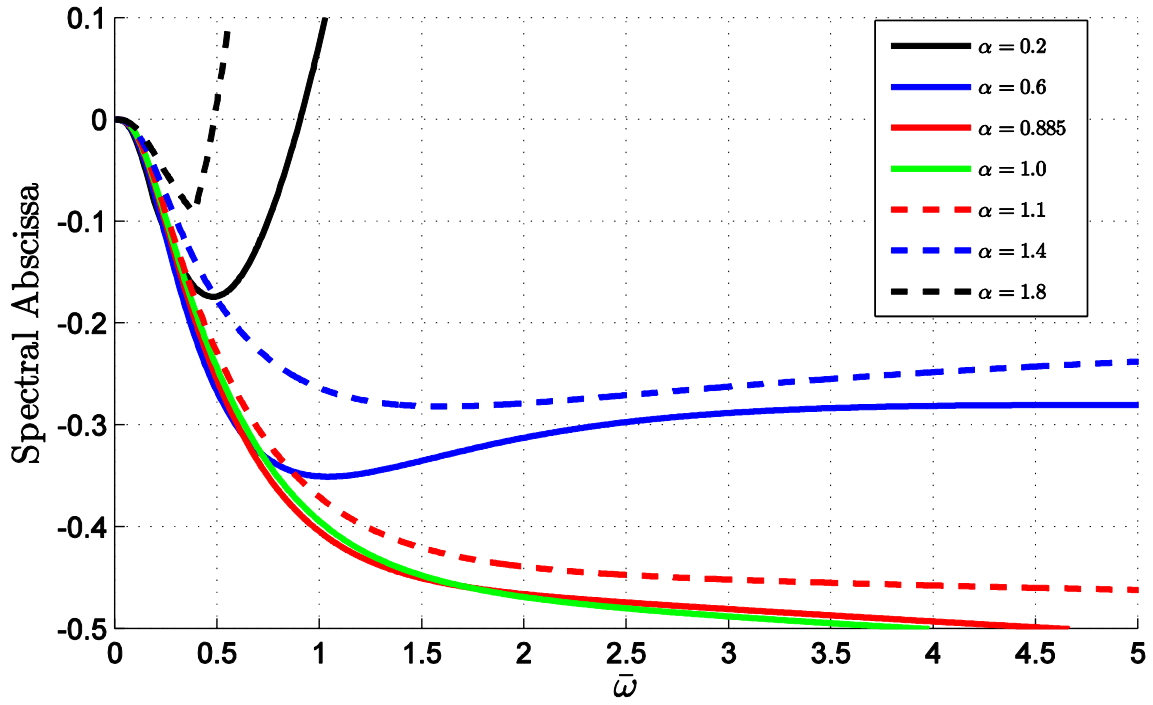


Figure 8. Spectral abscissa of the CS with respect to α for $l = 2$.

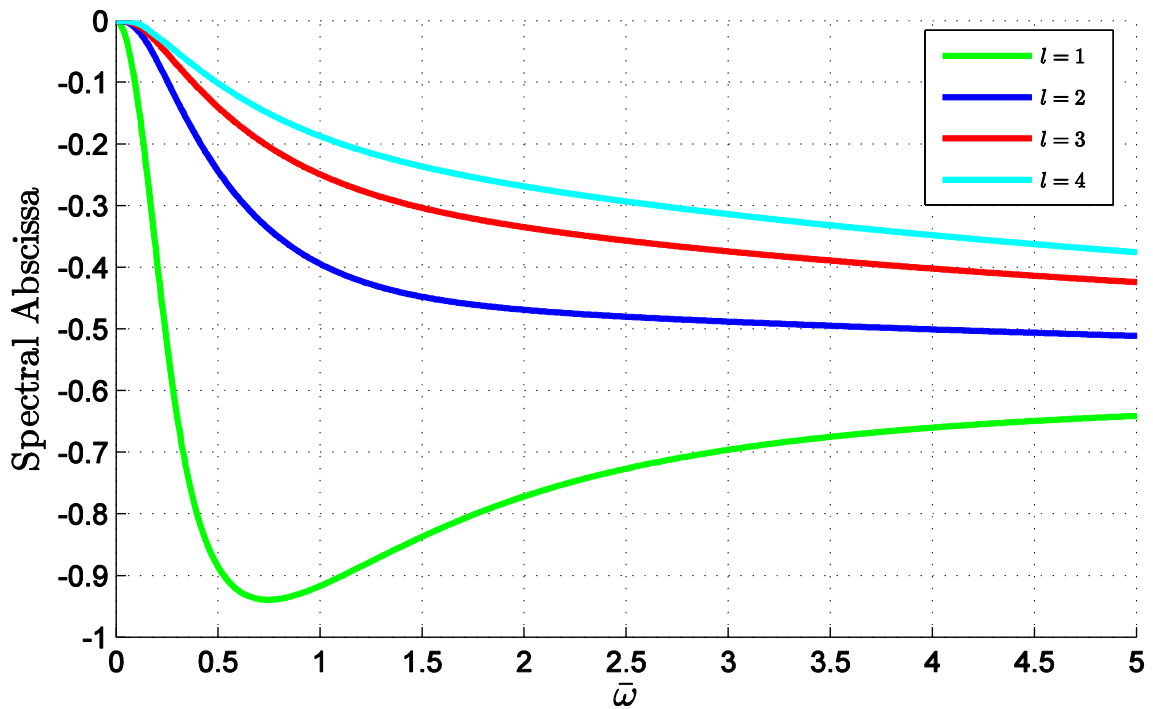


Figure 9. Spectral abscissa of the CS with respect to l for $\alpha = 1$.

spectral abscissa of the CS is getting closer to the imaginary axis as higher delay branches are chosen.

The design of the proposed DR approach is independent from the primary system similar to the classical DR method. Hence, the stability of the CS is also investigated for the proposed method by changing the damping ratio of the primary system. The spectral abscissa of the CS for primary structures with different damping ratios are presented in Fig. 10 where free parameters of the proposed approach are chosen as $\alpha = 1$ and $l = 2$.

It is determined that the stable operation range of the DR is extended with the proposed method comparing the results for the proposed method, presented in Fig. 10, with the classical DR methods (Fig. 3). Moreover, the spectral abscissa of the proposed method is mostly farther from the imaginary axis compared to the second delay branches of the classical methods.

Remark 4: The transcendental term in the characteristic equation of DR (31) drops since the delay is zero for $l = 1$ when the parameters in (30) are used. Then, applying the Routh Hurwitz method to investigate the stability of the given characteristic equation, the stability condition is easily obtained as

$$\frac{(\bar{c}_p + 2\zeta) + (\bar{c}_p - 2\bar{k}_p\zeta)}{\bar{m}_p} > \bar{\omega}^2. \quad (32)$$

5. EXPERIMENTAL VERIFICATION

An experimental setup is prepared to verify the theoretical results obtained in this study by using the Quanser© Active Suspension System as presented in Fig. 11. analogous to

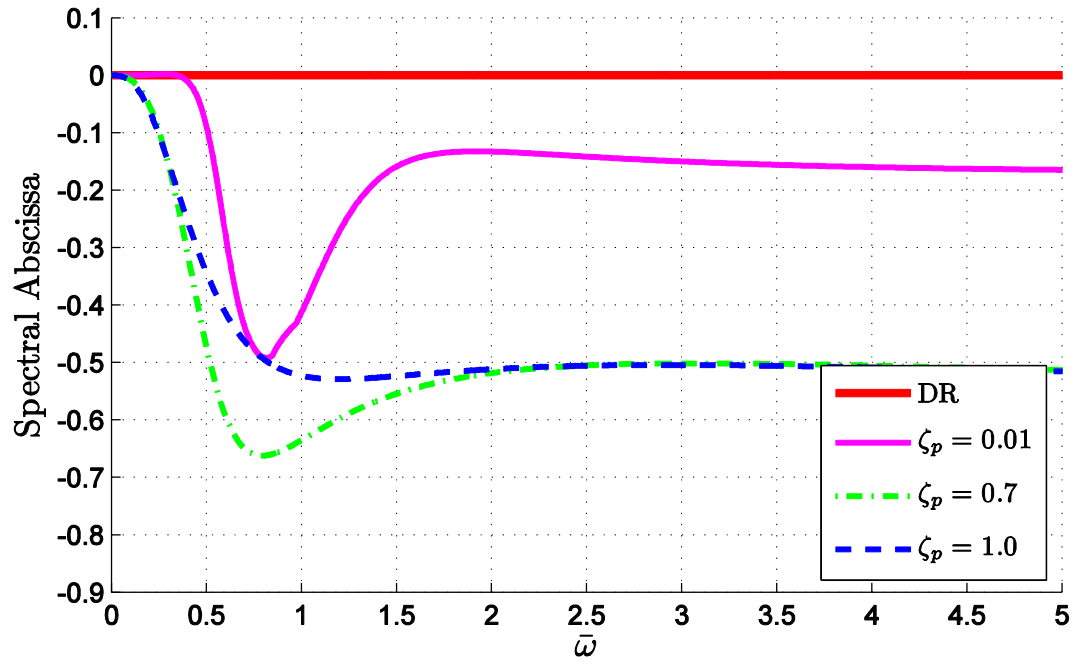


Figure 10. Spectral abscissa of the CS with respect to ζ_p ($\alpha = 1, l = 2$).

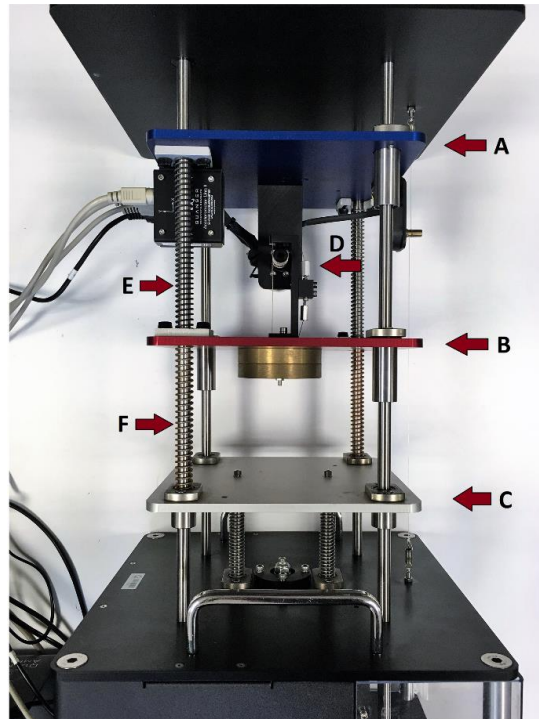


Figure 11. Experimental setup. (A: Absorber mass, B: Primary mass, C: Shaker, D: Actuator, E: Absorber spring, F: Primary spring)

Fig. 1 the red plate with the additional mass (B) is considered as the primary structure while the blue plate (A) is utilized as the absorber mass. A DC motor with a capstan mechanism (D) is used to actuate both of the plates. The vibrations are induced to the primary structure by shaking the grey plate (C) at the desired frequency. Physical parameters of the experimental setup are given as $m_p = 4.4 \text{ kg}$, $c_p = 5 \text{ kg s}^{-1}$, $k_p = 2500 \text{ N m}^{-1}$, $m_a = 2 \text{ kg}$, $c_a = 5.8 \text{ kg s}^{-1}$, $k_a = 900 \text{ N m}^{-1}$. The damping ratio and the natural frequency of the absorber with these parameters are determined as $\zeta = 0.0684$ and $\Omega = 3.3762 \text{ rad s}^{-1}$ respectively. Stability posture of the DR and CS for classical DR approaches are exhibited in Fig. 12.

Three different scenarios are constructed for the experimental validation of the theoretical findings through different vibration frequencies as:

1. $\bar{\omega} = 1$ which is the natural frequency of the DR.
2. $\bar{\omega} = 0.8$ where stable operation is not possible for any of the classical DR methods.
3. $\bar{\omega} = 1.481$ where stable operation is not possible for any of the classical DR methods using higher delay branches ($l > 1$).

The optimal α value that locates the spectral abscissa of the CS farthest from the imaginary axis for $\bar{\omega} = 1$ is found as 0.829 ($l = 2$) using the scheme presented in (18).

For the second and third scenario, α parameter is selected as $\alpha = 1$ while the second and third delay branches are utilized respectively. DR parameters are listed in Table 1 and experiment results of these scenarios are presented Fig. 13. Displacement of the

Table 1. The parameters of the DR in experimental setup

Excitation Frequency		DR Parameters							
ω (Hz)	$\bar{\omega}$	α	l	g_v	\bar{g}_v	g_p	\bar{g}_p	τ	$\bar{\tau}$
3.376	1.0	0.829	2	9.2884	0.2189	153.9	0.171	0.2539	0.012
2.7	0.8	1	2	5.8	0.1367	324.0	0.36	0.3702	0.0175
5	1.481	1	3	5.8	0.1367	-1073.9	-1.1932	0.2	0.0094

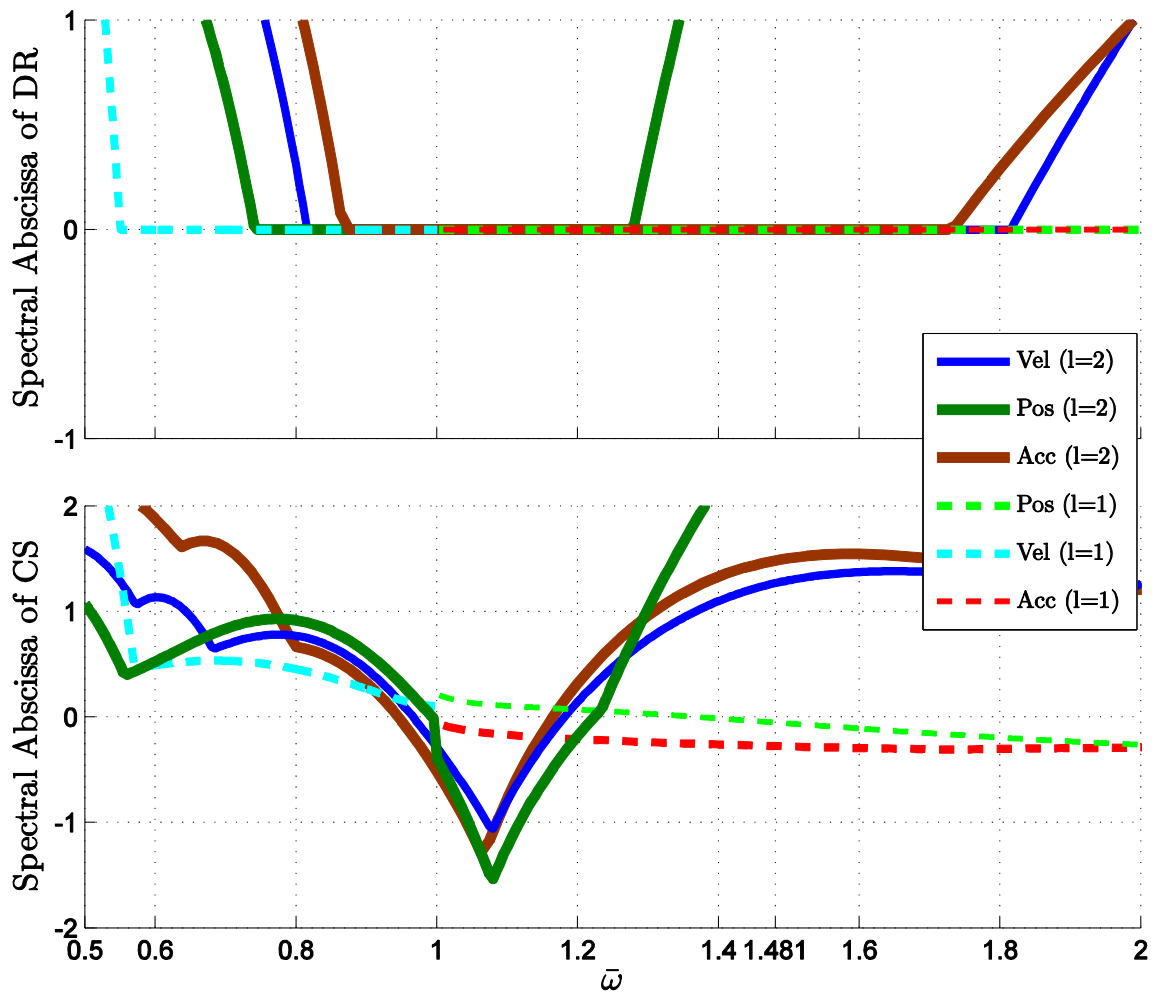


Figure 12. Spectral abscissa of the DR and CS with respect to changing excitation frequency.

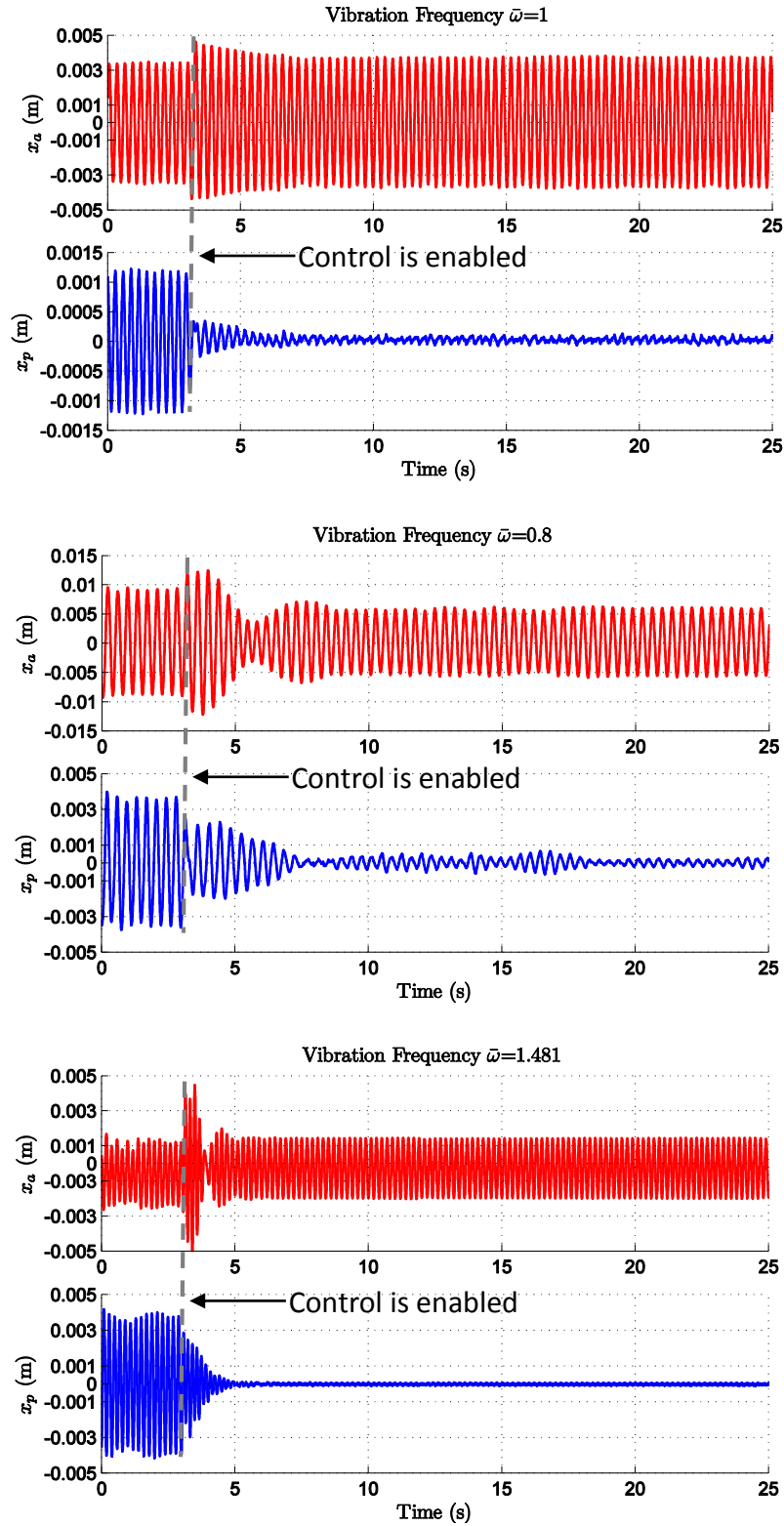


Figure 13. Experimental verification of the proposed method ($\bar{\omega} = 1$ top, $\bar{\omega} = 0.8$ middle, $\bar{\omega} = 1.481$ bottom).

shaker is set to 2 mm considering the physical limitations of the absorber ($\Delta x_a = 15\text{ mm}$). Note that the DRs are activated at $t = 3\text{ s}$ for all the scenarios.

Experimental results display that both DR and CS are stable for the given scenarios. Note that for this system, stable operation is not possible for $\bar{\omega} = 0.8$ using classical DR methods since CS is unstable. Moreover, the alternative approaches presented in [18] that also aims to extend the operable frequency range of the classical DR methods cannot provide stable operation for $\bar{\omega} = 0.8$. A similar situation also appears for $\bar{\omega} = 1.481$ as stable operation is only possible for the first delay branches of the DRs with position and acceleration feedbacks. Despite being stable theoretically, delay values regarding the first delay branches of the position and acceleration feedbacks are calculated as $\tau = 0.0056\text{ s}$ which is practically hard to implement as demonstrated in [18]. Meanwhile, feedback delay for the proposed approach is calculated as $\tau = 0.4\text{ s}$ for the second delay branch which is applicable practically and theoretically as seen from the experiment results.

Experiment results also indicate that the vibrations are suppressed within 5 seconds for the second and third scenarios. On the other hand, suppression quality is slightly reduced for $\bar{\omega} = 0.8$ due to physical constrains on the displacements of the plates of the experimental setup.

The parameters of control scheme are changed offline during the experiments for the sake of clarity of the Figure 13. Although it is cumbersome to obtain spectral abscissa of a transcendental equation real time, it is possible to precompute feedback delay and gains with a fine grid of the ω , α and then create a lookup table. If the system designer

keeps $\alpha = 1$ for all the operational region, only τ and g_p are computed which have almost no computational burden.

6. CONCLUSION

A modified DR approach with a combined feedback strategy, namely delayed velocity and non-delayed position feedback together, is presented. The non-delayed position feedback is used to manipulate the natural frequency of the DR artificially while the delayed velocity feedback is employed to oscillate the DR at the desired frequency to be suppressed on the primary structure. The position feedback gain is a freely assigned parameter which enables the designer to locate the rightmost root of the CS farthest in LHP for faster vibration suppression. An optimization approach is presented in this sense.

Besides, the proposed combined strategy with a free parameter determination provides an extended operable frequency range where DR vibration absorber is marginally stable. Extension of the operable frequency range also enables the selection of higher delay branches that offer larger τ values. Hence, upper bound of the delay parameter for the operation frequency due to the sampling time constraints of the implementation hardware is relaxed. The efficiency of the proposed method is presented with the stability analysis and experimental results.

ACKNOWLEDGMENT

The work of the second author was supported by the European Regional Development Fund under the project Robotics for Industry 4.0 (reg. no. CZ.02.1.01/0.0/0.0/15_003/0000470).

REFERENCES

- [1] Olgac, N., and Holm-Hansen, B.T., 1994, "A Novel Active Vibration Absorption Technique: Delayed Resonator," *Journal of Sound and Vibration*, **176**(1), pp.93-104.
- [2] Olgac, N., and Hosek, M., 1997, "Active Vibration Absorption Using Delayed Resonator with Relative Position Measurement," *Journal of Vibration and Acoustics*, **119**(1), pp.131-136.
- [3] Olgac, N., Elmali, H., Hosek, M., and Renzulli, M., 1997, "Active Vibration Control of Distributed Systems Using Delayed Resonator with Acceleration Feedback," *Journal of Dynamic Systems Measurement and Control*, **119**(3), pp.380-389.
- [4] Eris, O., Ergenc, A.F., and Kurtulan, S., 2015, "A Modified Delayed Resonator for Active Suspension Systems of Railway Vehicles," *IFAC-PapersOnLine*, **48**(12), pp.281-285.
- [5] Olgac, N., and Holm-Hansen, B.T., 1995, "Design Considerations for Delayed-Resonator Vibration Absorbers," *Journal of Engineering Mechanics*, **121**(1), pp.80-89.
- [6] Olgac, N., Elmali, H., and Vijayan, S., 1996, "Introduction to the Dual Frequency Fixed Delayed Resonator," *Journal of Sound and Vibration*, **189**(3), pp.355-367.
- [7] Olgac, N., 1996, "Single mass dual frequency fixed delayed resonator," *United States Patent* 5, 505, 282.
- [8] Renzulli, M., Roy, R.G., and Olgac, N., 1999, "Robust Control of the Delayed Resonator Vibration Absorber," *IEEE Transactions on Control Systems Technology*, **7**(6), pp.683-691
- [9] Jalili, N., and Olgac, N., 2000, "Identification and Retuning of Optimum Delayed Feedback Vibration Absorber," *Journal of Guidance Control and Dynamics*, **23**(6), pp.961-970.

- [10] Hosek, M., and Olgac, N., 2002, "A Single-Step Automatic Tuning Algorithm for the Delayed Resonator Vibration Absorber," *IEEE/ASME Transactions on Mechatronics*, **7**(2), pp.245-255.
- [11] Olgac, N., and Jalili, N., 1999, "Multiple Delayed Resonator Vibration Absorbers for Multi-Degree-of-Freedom Mechanical Structures," *Journal of Sound and Vibration*, **223**(4), pp.567-585.
- [12] Filipovic, D., and Olgac, N., 2002, "Delayed Resonator with Speed Feedback—Design and Performance Analysis," *Mechatronics*, **12**(3), pp.393-413.
- [13] Hosek, M., Elmali H., and Olgac, N., 1997, "A Tunable Torsional Vibration Absorber: The Centrifugal Delayed Resonator," *Journal of Sound and Vibration*, **205**(2), pp.151-165.
- [14] Kammer, A.S., and Olgac, N., 2016, "Delayed-Feedback Vibration Absorbers to Enhance Energy Harvesting," *Journal of Sound and Vibration*, **363**, pp.54-67.
- [15] Tootoonchi, A.A., and Gholami, M.S., 2011, "Application of Time Delay Resonator to Machine Tools," *The International Journal of Advanced Manufacturing Technology*, **56**(9-12), pp.54-67.
- [16] Eris, O., Ergenc, A.F., and Kurtulan, S., 2014, "Use of Non-Identical Multiple Delayed Resonators in Active Suspension Systems of Railway Vehicles," *IEEE International Conference on Control System Computing and Engineering*, Penang, pp.588-591.
- [17] Vyhlidal, T., Olgac, N., and Kucera, V., 2014, "Delayed Resonator with Acceleration Feedback—Complete Stability Analysis by Spectral Methods and Vibration Absorber Design," *Journal of Sound and Vibration*, **333**(25), pp.6781-6795.
- [18] Pilbauer, D., Vyhlidal, T., and Olgac, N., 2016, "Delayed Resonator with Distributed Delay in Acceleration Feedback—Design and Experimental Verification," *IEEE/ASME Transactions on Mechatronics*, **21**(4), pp.2120-2131.
- [19] Eris, O., and Ergenc, A.F., 2016, "Delay Scheduling for Delayed Resonator Applications," *IFAC-PapersOnLine*, **49**(10), pp.77-81.
- [20] Breda, D., Maset, S., and Vermiglio, R., 2014, *Stability of Linear Delay Differential Equations: A Numerical Approach with MATLAB*, Springer, New York, USA. ISBN: 9781493921072
- [21] Vyhlidal, T., and Zitek, P., 2009, "Mapping Based Algorithm for Large-Scale Computation of Quasi-Polynomial Zeros," *IEEE Transactions on Automatic Control*, **54**(1), pp.171-177.

[22] Wu, Z., and Michiels, W., 2012, "Reliably Computing All Characteristic Roots of Delay Differential Equations in a Given Right Half Plane Using a Spectral Method," *Journal of Computational and Applied Mathematics*, **236**(9), pp.2499-2514.

[23] Olgac, N. and Sipahi, R., 2002, "An exact method for the stability analysis of time-delayed linear time-invariant (LTI) systems," *IEEE Transactions on Automatic Control*, **47**(5), pp.793-797.

[24] Rekasius Z.V., 1980, "A stability test for systems with delays," *Proceedings of the Joint Automatic Control Conference*, Paper TP9-A.

[25] Rivaz, H. and Rohling, R., 2007, "An Active Dynamic Vibration Absorber for a Hand-Held Vibro-Elastography Probe," *Journal of Vibration and Acoustics*, **129**(1), pp.101-112.